Investigating the Co-precessing Frame Approximation for Binaries on Eccentric Orbits

Sam Johar
Mentors: Lucy Thomas and Taylor Knapp
(Dated: November 4, 2025)

Quasi-circularity has historically been assumed for detected gravitational waves from black hole compact binary coalescences. As low-frequency detector sensitivity improves, we expect to detect these systems farther from merger, before eccentricity has been radiated away. To analyze these signals, we will need well developed and robust eccentric models. Few existing models incorporate precession and eccentricity together as the resulting waveforms are complicated and difficult to model. The co-precessing frame is one tool that simplifies precessing waveforms by creating a reference frame in which the z-axis is always aligned with orbital angular momentum, a transformation that is well-studied for quasi-circular systems and often used to create precessing waveform models. Here we evaluate the co-precessing frame approximation for eccentric and precessing numerical relativity simulations. We find that while shifting to the co-precessing frame counteracts amplitude modulation in the waveform envelope, mode asymmetries remain in the untwisted waveform. We also begin a preliminary analysis of possible shifts in eccentricity and other waveform dynamics due to the co-precessing frame transformation by generating eccentric SEOBv5EHM waveforms. The determination of which precession features linger in the co-precessing frame will aid in future efforts to construct a robust waveform model that includes the effects of both eccentricity and precession.

I. INTRODUCTION

Analysis of current LIGO data assumes that the orbit of a binary black hole (BH) system is quasi-circular. However, as detector sensitivity increases, we are more likely to begin observing eccentricity in detected waveforms. Part of the reason that LIGO detectors have not yet identified a non quasi-circular system is that eccentric binaries tend to circularize over time as gravitational waves emitted by the system radiate away eccentricity by removing excess angular momentum from the system. This circularizing effect can be seen in Figure 1, which depicts the inspiral of a low eccentricity waveform model. As detectors become more sensitive in the low frequency range (20Hz-50Hz), the inspirals of detected compact binary coalescences (CBCs) will be better resolved, giving us a better chance of seeing eccentricity before it has been radiated away. Additionally, now that we have identified many CBCs and analyzed them under the assumption of quasi-circularity, we are in a better position to relax this assumption going forward.

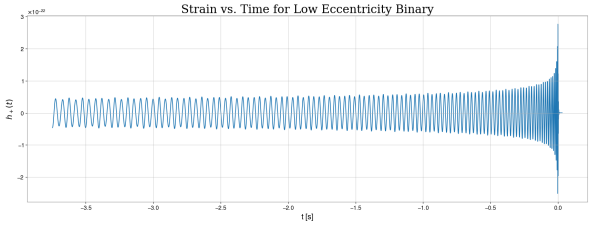

FIG. 1. Plus polarization of strain over time for the inspiral of a BH binary with 0.05 eccentricity. At the beginning of the inspiral, the periodic higher amplitude "knocking" characteristic of an eccentric system is clearly visible. One such knock can be seen just before the -3.5 second mark. However, these knocks become less clearly distinguishable throughout the inspiral. This waveform was generated with the LIGO Algorithm Library Simulation (LALSimulation) code package [1].

Binary black hole systems form in two main ways: isolated formation and dynamical capture. Isolated binaries are systems where the two bodies were orbiting each other in a binary before becoming black holes, while dynamical systems form when two pre-existing black holes approach each other, usually in a globular cluster, and are caught in each others' gravitational pull [2]. In isolated systems, we expect the orbit to be quasi-circular. By quasi-circular, we mean that over each orbital period the system's orbit is well approximated by a circle. Over time, the radius of the circle gradually decreases due to the emission of gravitational waves, but for quasi-circular systems the timescale of this decrease in radius is much longer than the orbital period. However, we expect that dynamical systems could have eccentric orbits, in part because the binary will not have had as much time to radiate away eccentricity. Thus, detecting eccentric waveforms would provide evidence towards such systems being formed via dynamical capture. Modelling eccentricity allows researchers to relax the assumption of quasi-circularity and will ensure that the tools exist to analyze eccentric waveforms when we eventually observe them.

Eccentricity (e) varies from 0 to 1 for bound systems, with e = 0 representing a circular orbit and e = 1 a parabolic orbit. In a quasi-circular orbit, each black hole has a constant angular velocity throughout one orbit. However when e > 0 and the orbit is elliptical, a black hole's angular velocity varies depending on the location in its orbit. At the point where the two black holes are closest together, known as **periastron**, the black holes travel with the fastest angular velocity and emit the highest amplitude and highest frequency GWs. Conversely, their angular velocity is slowest when they are farthest away from each other at **apastron**, and they

emit lower amplitude GWs. These amplitude and frequency changes modulate the signal, creating periodic "knocks" at periastron[3]. Binaries with elliptical orbits will also experience **periastron precession**, an effect predicted by general relativity wherein an object's orbit itself precesses around the focus of its orbital ellipse within the orbital plane. This precession is due to ellipticity, and is not related to spin.

Taking into account the spins of the black holes in a CBC further complicates the observed GW. General relativity predicts that spinning objects affect the curvature of spacetime by "dragging" the space around them[4]. In a binary black hole system, we denote the orbital angular momentum vector $\vec{L}$. This vector is by definition always perpendicular to the instantaneous plane of orbit. When the spins of the black holes are parallel or anti-parallel to $\vec{L}$, the system has **aligned spins** and both the spins and orbital angular momentum remain fixed in direction[5]. Systems with aligned spins have been well modelled and investigated[6].

However, if the spins are not aligned with $\vec{L}$, the system is complicated by a precession effect known as **Lense-Thirring Precession**, which has been observed in in some detected binary black hole mergers. Due to general relativity, a spinning black hole will drag the space around it within the plane of orbit, affecting the GWs it emits. This dragging effect creates spin-orbit and spin-spin couplings, leading both the orbital plane (and thus $\vec{L}$) and the spins of the black holes themselves to precess[4]. Precession leads to modulation of the signal's amplitude and frequency as the alignment of the incoming GW with respect to the detector changes with $\vec{L}$, an effect that is demonstrated by Figure 2. The phase of the precessing waveform is also modulated, though this effect is more difficult to observe in the plot. Figure 3, which is Figure 1 in Shaikh et al. 2025 [7], uses numerical relativity (NR) simulations to depict the effects of eccentricity and precession on a waveform in the time-domain.

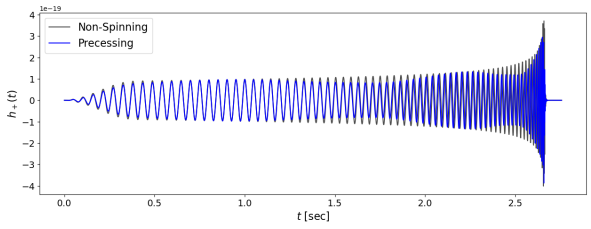

FIG. 2. Plus-polarization of strain over time for the inspiral of a precessing waveform (blue) and non-precessing waveform (grey). Amplitude modulation of the precessing waveform is clearly visible in contrast to the smooth amplitude increase in the non-precessing waveform. The two waveforms are roughly the same length, indicating that precession does not affect inspiral duration. Both waveforms were generated with LALSimulation [1].

Another effect caused by precession is mode asymmetry. In a non-precessing waveform, the following equation holds for each (ℓ,m) mode:

$$h^{\ell,m} = (-1)^{\ell}\bar{h}^{\ell,-m}. \tag{1}$$

[8] Thus, for a non-precessing system, the amplitudes of corresponding (ℓ,m) and (ℓ,-m) modes are the same. However, in a precessing system, spin-orbit couplings between the black holes and the orbital plane cause a breakdown in these symmetries on the orbital timescale as the orbital plane itself is precessing *during* each orbit and thus symmetry across the orbital plane during each orbit is lost.

One tool to simplify the complex waveforms from precessing systems is the **co-precessing frame** ([9][10][11]). The co-precessing frame is the reference frame that rotates with $\vec{L}$ such that $\vec{L}$ is always in the +z direction. Within the co-precessing frame, the seven-dimensional parameter space of a precessing system (mass ratio + the three spin vector components for both black holes) is reduced to a three-dimensional space on waveforms that do not precess (Parameters of this three-dimensional space are mass ratio, and spin components parallel to $\vec{L}$ for each black hole). One way to shift into this frame is to characterize the precessing system by describing $\vec{L}$'s position with respect to each axis with three time-dependent rotation angles. Of those three angles, $\beta(t)$, the angle between $\vec{L}$ and the +z axis in the lab frame, is the most characteristic of precession effects. Shifting into the co-precessing frame forces $\beta(t) = 0$, simplifying the system as described by Schmidt et al [6]. We utilize the minimal rotation condition version of the co-precessing frame, which enhances this technique by uniquely defining the rotation operator as described in Boyle et al. 2011 [12].

The co-precessing frame approximately removes precession effects, leaving a waveform that resembles the signal from a non-precessing system. However, while shifting to this frame greatly reduces effects such as amplitude modulation by ensuring that $\vec{L}$ and $\hat{z}$ are always aligned, some precession effects remain. In particular, the mode asymmetries created by precession are features that cannot be removed with the co-precessing frame transformation (nor in any other frame), as proven in Section IIB of Boyle et al. 2014 [8].

Inspiral-merger-ringdown (IMR) models for quasi-circular precessing systems are mature and have been used extensively for GW data analysis. IMR models with eccentric inspirals have also been used for data analysis more recently, but these models do not include eccentricity in the merger or ringdown phase—a fairly accurate approximation as a binary typically circularizes through gravitational radiation before the merger stage. Eccentric and precessing inspiral models using Post-Newtonian (PN) approximations exist, but no well-reviewed or tested eccentric and precessing IMR models exist as of yet. The closest current model [13], which is in early stages of development, has not yet been reviewed by the LVK collaboration for use in analysis. This model

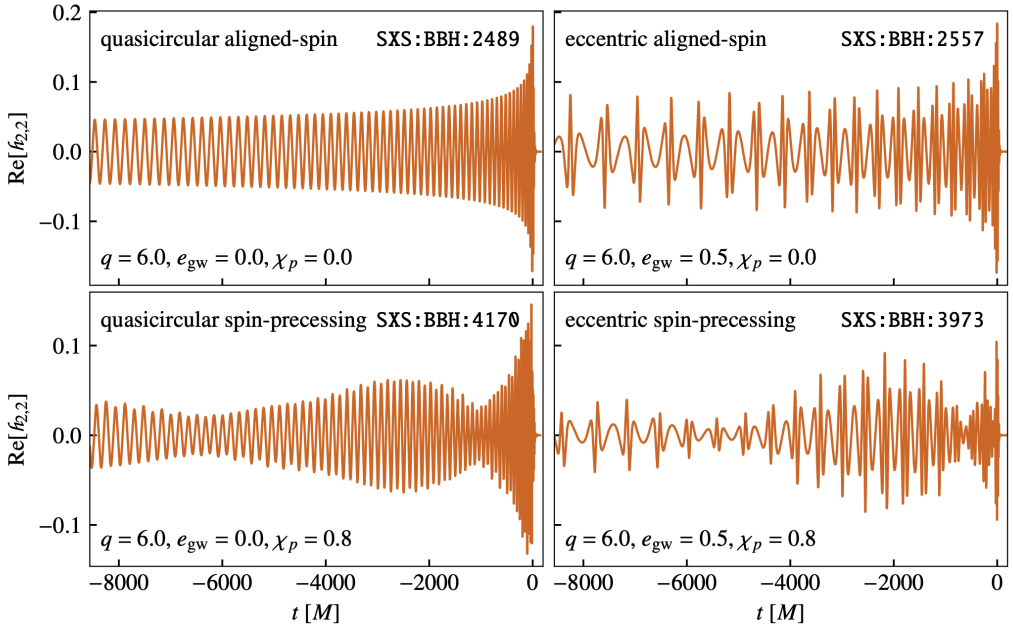

FIG. 3. Effect of eccentricity and precession individually and in combination on (2,2) mode of time-domain waveform. Figure accessed from [7].

uses the co-precessing frame approximation to construct eccentric and precessing IMR waveforms. However, while the impacts of the co-precessing frame on quasi-circular binaries has been widely studied and used extensively in precessing waveform models, this "untwisting" effect has not been well studied for waveforms that are both eccentric and precessing.

Our objective is to study the co-precessing frame as a tool to remove dominant precession effects for eccentric waveforms. We hope to determine the accuracy of this approximation in removing precession effects from eccentric waveforms by comparing untwisted eccentric precessing and eccentric non-precessing waveforms. In particular, we will try to explain and characterize flaws in this approximation by studying mode asymmetries in the waveforms. We begin with a brief overview of our motivations in Section II. Keeping these goals in mind, we introduce our methods in Section III. In Section IVA, we present an initial analysis of the effect of changing five parameters (total mass, mass ratio, aligned spin, precession, and eccentricity) on a waveform, as well as the effect of precession, eccentricity, and mass ratio on mode hierarchy. In Section IVB, we present results from our exploration of the motion of orbital angular momentum vector $\vec{L}$ for waveforms of varying eccentricity and precession. In Section IVC, we begin investigating the co-precessing frame by transforming two NR waveforms and comparing the resulting time-domain waveform and waveform modes to their inertial frame counterparts to observe the effect of the transformation. We build on this investigation in Section IVD, where we compare untwisted eccentric precessing waveforms to eccentric non-precessing waveforms to show that the co-precessing frame does not affect mode asymmetries. Section V details our proposed next steps for this project, both immediate goals like quantitative comparisons and long-term plans to construct a robust eccentric precessing waveform model using NR surrogates.

II. OBJECTIVES

Determining a relationship between eccentric and precessing waveforms and quasi-circular eccentric waveforms through the co-precessing frame allows us to construct quasi-circular waveform models that include eccentricity and precession. If we are able to determine a map between precessing and non-precessing *eccentric* waveforms, this future model could begin by creating non-precessing eccentric waveforms, then add in precession by "twisting" up with the inverse of the co-precessing frame approximation—an easier alternative to the complicated physics needed to model eccentric and precessing waveforms otherwise. We could then add in effects such as mode asymmetries, which our study shows are not created by the co-precessing frame transformation alone. Having such a model will increase our ability to identify future GW detections as eccentric and precessing. Additionally, this work will increase our understanding of the co-precessing frame and waveform eccentricity for CBCs.

III. METHODS

We begin by sorting through the SXS catalog [14] to find all non-precessing Numerical Relativity (NR) waveforms simulations, both eccentric and quasi-circular. For non-precessing waveforms, the co-precessing frame transformation should have no effect as the orbital angular momentum is already aligned with the z-axis throughout the inspiral. To confirm this lack of effect, we untwist each non-precessing waveform to the co-precessing frame and take the mismatch between the original and untwisted waveforms. The mismatch is an inner product between two frequency-domain waveforms varying from zero when the waveforms are identical, to one when they are entirely orthogonal. Taking checking if these mismatches are low, we can determine if isolated eccentricity features remain unaffected by the co-precessing frame transformation, as we would expect.

We then move to considering precessing simulations. We identify the 27 undeprecated eccentric and precessing NR simulations by their parameters at the simulation reference time, taking minimum eccentricity to be considered eccentric to be e=0.01, and identify non-precessing NR simulations as "matches". These match waveforms have no precession, but otherwise the same parameters as the original eccentric and precessing waveforms. We then transform SXS simulations into the co-precessing frame using the scri code [11], and compare each resulting "untwisted" waveform to its non-precessing counterpart. This comparison is done qualitatively (by eye looking at time-domain plots of strain and modes) and quantitatively (by calculating the mismatch between each pair of waveforms). By comparing each "untwisted" waveform to an eccentric non-precessing counterpart, both qualitatively and quantitatively, we can determine how well the transformation removes precession effects. In particular, we can determine which effects it does *not* remove, especially by examining the presence of mode asymmetries in "untwisted" waveforms as compared to non-precessing ones.

Due to the sparse parameter space coverage of precessing/eccentric NR simulations, there are a limited number of matches in the SXS catalog, limiting the above analysis. To navigate this issue, we use the SEOBv5EHM model (discussed in [15]) for eccentric non-precessing waveforms to generate matches for the 27 eccentric precessing NR waveforms. These matches are generated with a code that, given an eccentric precessing SXS waveform, repeatedly creates v5EHM models, varying starting orbital frequency and eccentricity until the time-domain mismatch between the two waveforms is minimized. We then compare the eccentricities of the two waveforms to determine if the co-precessing frame transformation affects a waveform's eccentricity, rather than just removing precession effects.

IV. RESULTS

We begin by changing different parameters to observe the resulting effects on GWs. Our observations from this analysis are discussed in Section IV A 1. We gain initial familiarity with the dynamics of eccentric precessing waveforms using an orbit-averaged PN code [16], making plots to observe how eccentricity and precession affect their inspirals in Section IV A 2. In Section IV B we investigate the mismatches between twisted and untwisted non-precessing waveforms, both quasi-circular and eccentric. In Section IV C, we detail our investigation of the parameters and characteristics of the 27 existing eccentric precessing NR waveform simulations, going through one comparison between an inertial and co-precessing frame waveform that reveals mode asymmetries. Finally, we discuss our first few preliminary results from generating v5EHM comparisons for eccentric precessing NR simulations in Section IV D.

A. Building Intuition

1. *Effect of Changing Parameters on Time-Domain Waveforms*

Parameter	**Effect of Increasing Parameter on Time-Domain Waveform**
Total Mass	Inspiral shortens and amplitude increases
Mass ratio	Inspiral lengthens and amplitude decreases
z-axis spin	Inspiral lengthens
Precession	Amplitude and frequency modulate
Eccentricity	Inspiral shortens, amplitude (at periastron) increases, "knocking" effect (uneven amplitude per period)

TABLE I. Summary of investigation into effect of increasing five parameters on time-domain waveforms. Investigation run by creating waveforms with PN code [16].

We present our findings from changing five parameters in Table I. We also present findings for how changing eccentricity and precession in particular affects mode hierarchy in Table II, and a corresponding plot in Figure 4. In our study, we primarily work with time-domain

Parameter	**Effect of Parameter on Mode Hierarchy**
Control (Non-spinning, quasi-circular, q = 1)	(2,2) mode is strongest, (2,1) and (3,3) modes are zero.
Precession	Adds power to (2,1) mode.
Eccentricity	Adds power to (3,3) and (2,1) modes.
Mass ratio	Adds power to (3,3) mode.

TABLE II. Effect of precession, eccentricity, and mass ratio on waveform mode hierarchy. Results for first three rows are displayed in Figure 4.

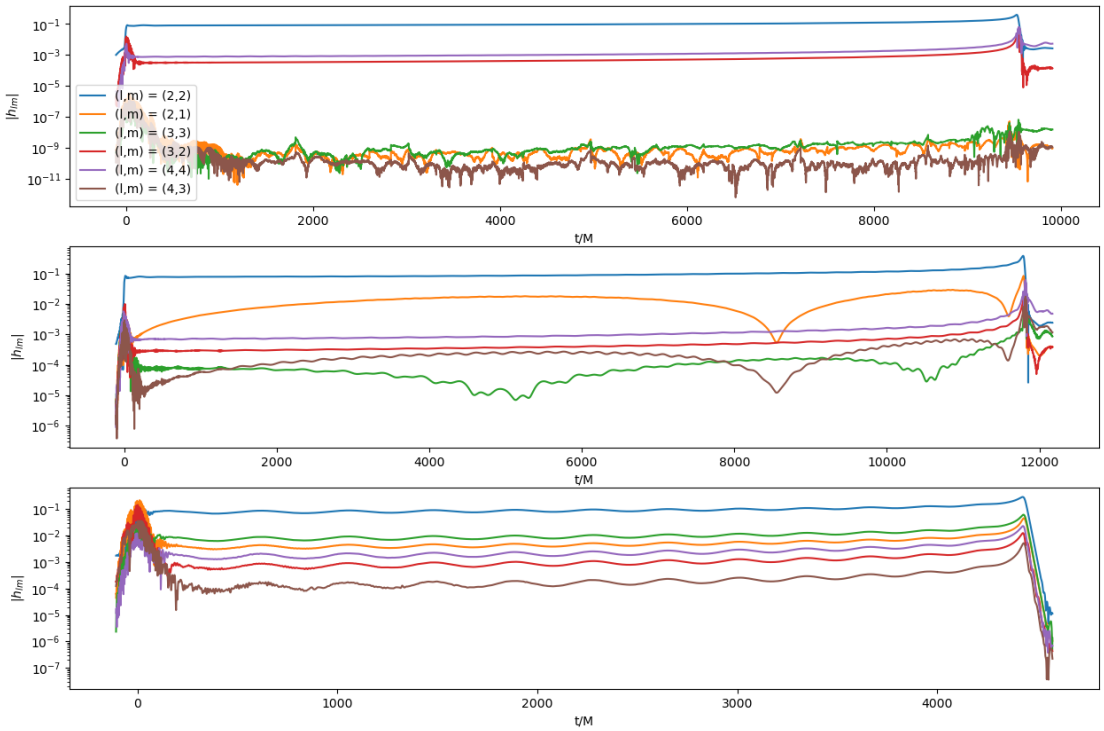

FIG. 4. Strain vs. time for six modes in control simulation, eccentric simulation, and precessing simulation. The mode hierarchy for the control simulation in order of decreasing amplitude is (2,2) (4,4) (3,2) (3,3) (2,1) (4,3). The precessing waveform adds power to the (2,1) mode, which becomes the second strongest. The eccentric waveform adds power to the (3,3) and (2,1) modes, which become the second and third strongest respectively. Plots were generated using NR simulations from SXS catalog[14].

waveforms and waveform modes. Thus, by studying the effects of changing the following parameters on the visual appearance of a waveform, we gain insight into the expectations for such waveforms, and an intuition for which effects result in which features on a signal.

2. *PN Investigation of Eccentric and Precessing Waveforms*

Using the eccprec PN code, we generate waveforms with varying precession and eccentricity respectively. As this code is orbit-averaged, the dynamics it outputs are missing complexity on the orbital timescale, making it difficult to fully analyze eccentric precessing waveforms with this code. However, it presents a computationally inexpensive way to model the macro shape of dynamics without orbital effects. In particular, we use this code to plot β(t), which is the angle of the orbital angular momentum $\vec{L}$ from the z-axis as a function of time (assuming $\vec{L}$ begins aligned with **z**). Figure 5 depicts the effect of increasing misaligned spin upon β(t), showing how systems with higher misaligned spin take the same amount of time to merge, but their orbital planes precess at a greater angle around total angular momentum $\vec{J}$. Figure 6 shows how $\beta(t)$ varies with eccentricity, with higher eccentricity systems merging faster and having higher amplitudes.

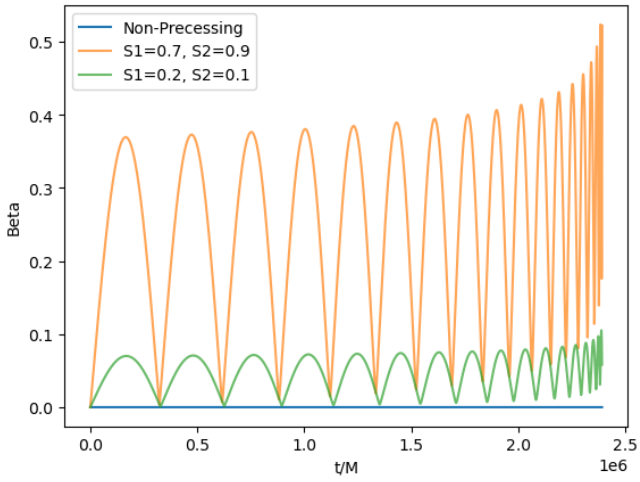

FIG. 5. $\beta(t)$ (Angle of $\vec{L}$ from $\hat{z}$) for three systems with varying precession. All spins in -x direction, and all waveforms equal mass with $e = 0.1$. The non-spinning waveform (blue) has $\beta = 0$, indicating no precession. The mildly spinning system (green) precesses at a lower angle than the highly spinning (orange). The lower envelope of each line is total angular momentum $\vec{J}(t)$, which diverges farther from $\hat{z}$ as precession increases. Waveforms generated with PN code [16] using $f_{start} = 10$ Hz.

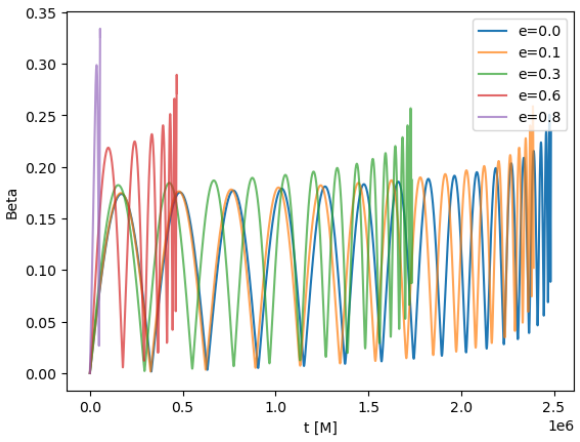

FIG. 6. $\beta(t)$ for five systems with varying eccentricity. All waveforms are from equal mass systems with $S_{1_x} = -0.25$ and $S_{2_x} = -0.5$, and all other spin components zero. More eccentric systems merge faster and reach higher precession angles. The lower envelope of each line is total angular momentum $\vec{J}(t)$, which does not appear to vary with eccentricity. Waveforms generated with PN code [16] using $f_{start} = 10$ Hz.

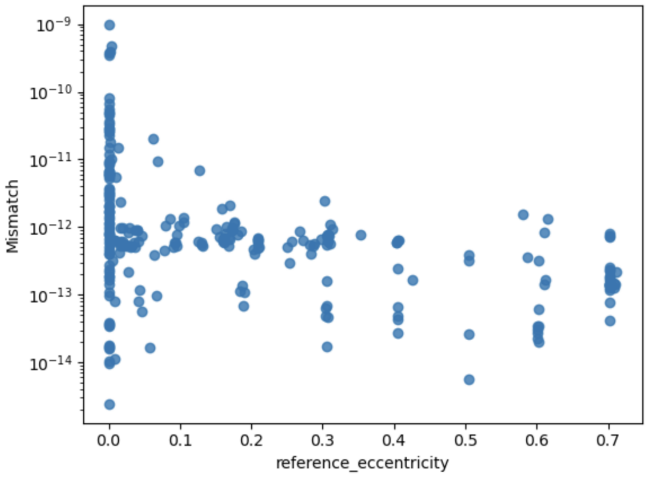

FIG. 7. Mismatch vs. eccentricity for NR non-precessing waveforms. R^2=0.172 and p=4.61e-12, indicating lack of correlation between both factors. Mismatches are negligible, indicating all waveforms compared are almost identical.

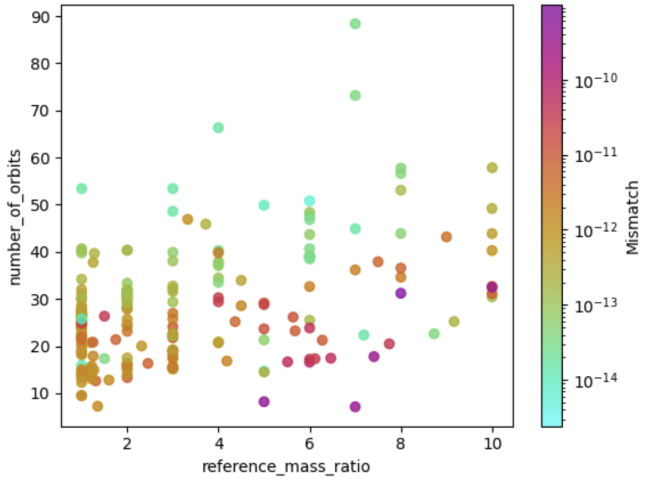

FIG. 8. Number of orbits vs. mass ratio with mismatch colorbar for NR non-precessing waveforms. For higher numbers of orbits, mismatch decreases, however there is little correlation between mismatch and mass ratio. Relationship to number of orbits suggests influence from NR simulation noise, rather than physical properties.

B. Non-Precessing NR Co-precessing vs. Inertial Frame Comparisons

By definition, the co-precessing frame and inertial frame should be identical for non-precessing waveforms. We test this hypothesis by taking mismatches between inertial and untwisted non-precessing waveforms, with results displayed in Figure 7. We find negligible mismatches on the order of $< 10^{-9}$, indicating that, as expected, the non-precessing NR waveforms are functionally identical in the inertial and co-precessing frames. Additionally, we found a correlation between mismatch and number of orbits, but not physical properties such as mass ratio (see Figure 8), suggesting that slight discrepancies between inertial and co-precessing frame waveforms are a result of NR simulation resolution limits and simulation noise. This analysis validates scri's ability to locate the co-precessing frame regardless of isolated eccentricity effects. However, it does not account for effects from eccentricity/precession interplay, which are unique to precessing systems. To address this issue, we move to comparisons with precessing NR simulations.

C. Precessing NR vs. Non-Precessing Match Comparisons

By filtering the SXS catalog we find 28 waveforms that are both eccentric and precessing, or 27 waveforms if we remove one which is deprecated (replaced with a newer version, and thus should not be used for analysis). We define eccentric to mean $e > 0.01$ and precessing to mean $\chi_{1_\perp} + \chi_{2_\perp} > 0.05$, as measured at the simulation reference time. We use scri to untwist these waveforms to the co-precessing frame and examine the results. In particular, we begin by qualitatively checking that the transformation decreases precession effects by comparing mode strength in the inertial and co-precessing frames, as depicted for SXS:BBH:3725 in Figure 9. We find that transforming to the co-precessing frame does dampen the (2,1) mode, making the waveform closer to one from a non-precessing system. We start by focusing on SXS:BBH:0088, which is an equal mass system with an eccentricity of 0.074 and one black hole spinning with $\chi_p = 0.5$. We plot the waveform from an edge-on view, as this perspective should yield no cross

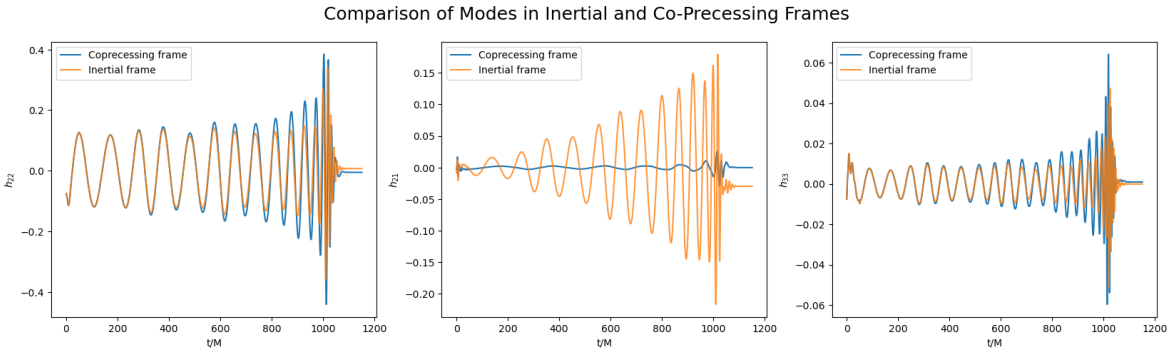

FIG. 9. Strain of (2,2) (2,1) and (3,3) modes over time in inertial (orange) and co-precessing (blue) frames for SXS:BBH:3725, a strongly eccentric and precessing waveform. In the co-precessing frame, the (2,1) mode is dampened to an amplitude much closer to what one would expect from a non-precessing waveform. As power is taken away from the (2,1) mode, the (2,2) and (3,3) modes gain power. Additionally, the amplitude increase of the (2,2) mode as the system approaches merger is smooth (apart from knocks due to eccentricity) in the co-precessing frame. Waveforms accessed from the SXS Catalog [14].

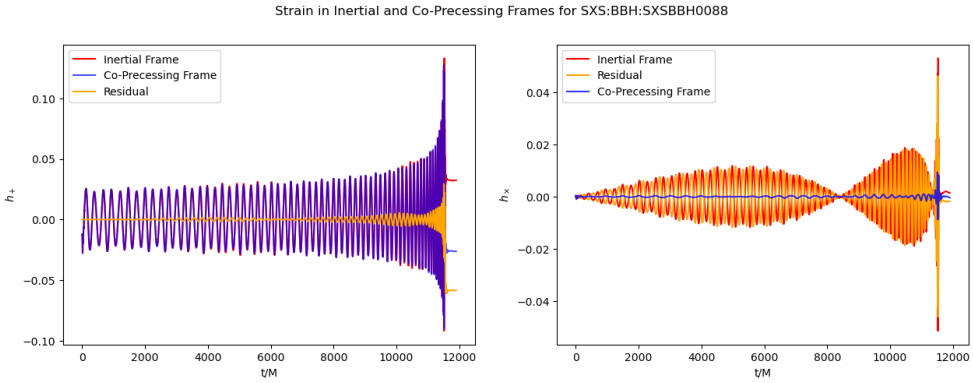

FIG. 10. Strain plus and cross polarization over time in inertial (red) and co-precessing (blue) frames for SXS:BBH:0088, plotted with the residual of those two quantities as a function of time. Waveforms accessed from the SXS Catalog [14].

polarization strain in a non-precessing waveform (Figure 10). The transformation to the co-precessing frame does flatten the cross polarization of the waveform to almost zero. The effect on the plus polarization is more difficult to see, but the residual shows how the waveform's amplitude is smoothed out in the co-precessing frame.

We implemented a code that filtered the entire SXS catalog to find "matches" to the 27 eccentric precessing waveforms. On our first run, we set the following parameters to be considered a match, where the "ep" supscript denotes eccentric precessing waveforms and the "match" subscript denotes a corresponding eccentric non-precessing waveform:

$$
\begin{aligned}
|\chi_{\mathrm{eff}_{ep}} - \chi_{\mathrm{eff}_{\mathrm{match}}}| &< 0.1 \\
|q_{ep} - q_{\mathrm{match}}| &< 0.4 \\
|\Omega_{ep} - \Omega_{\mathrm{match}}| &< 0.0005 \\
0.7 < \frac{e_{ep}}{e_{\mathrm{match}}} &< 1.3 \\
|\chi_{1_{\perp_{\mathrm{match}}}} + \chi_{2_{\perp_{\mathrm{match}}}}| &< 0.01
\end{aligned}
$$

With these condition, we find only one match: SXS:BBH:0088 and SXS:BBH:2580. We implement a second set of matching criteria using mean anomaly (as shown below) to find more matches:

$$
\begin{aligned}
|\chi_{\mathrm{eff}_{ep}} - \chi_{\mathrm{eff}_{\mathrm{match}}}| &< 0.1 \\
|q_{ep} - q_{\mathrm{match}}| &< 0.4 \\
|N_{ep} - N_{\mathrm{match}}| &< 15 \\
|\ell_{ep} - \ell_{\mathrm{match}}| &< \frac{\pi}{8} \\
0.6 < \frac{e_{ep}}{e_{\mathrm{match}}} &< 1.4 \\
|\chi_{1_{\perp_{\mathrm{match}}}} + \chi_{2_{\perp_{\mathrm{match}}}}| &< 0.01
\end{aligned}
$$

With these criteria, we identify two more matches: a new match for SXS:BBH:0088 in SXS:BBH:2519, and an entirely new pair between SXS:BBH:3974 and SXS:BBH:2581. A visual depiction of the parameters of each match is shown in Figure 12. We take the mismatches between each of these pairs of waveforms both

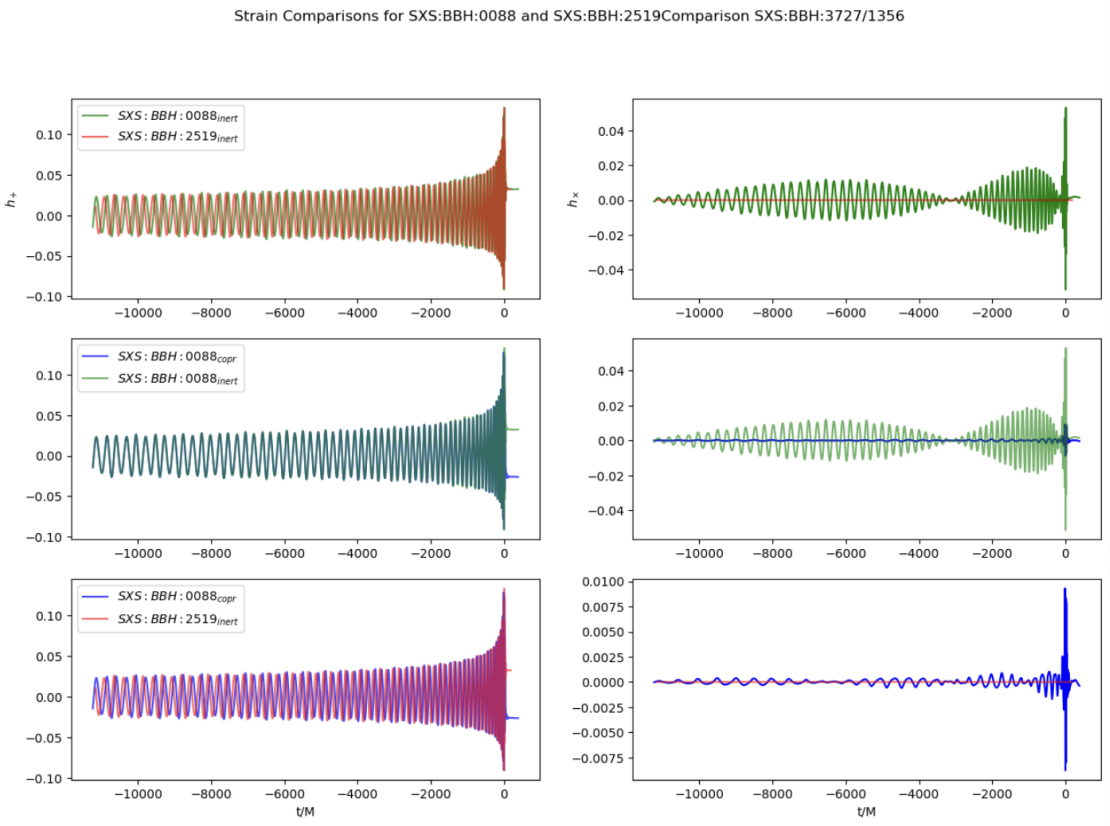

FIG. 11. Plus and cross polarization of strain over time for SXS:BBH:0088 in inertial (orange) and co-precessing (purple) frames and SXS:BBH:2519 (grey). Darker shades correspond to (2,+2) mode, and lighter (2,-2) mode. In the co-precessing frame, the two simulations' plus polarizations are similar, but small oscillations with modulated amplitudes on the precession timescale are visible in the cross polarization of SXS:BBH:0088 that are not present in its non-precessing counterpart. There are some precession effects that the co-precessing frame transformation does not remove. Waveforms accessed from the SXS Catalog [14].

Eccprec sim	Ecc non-prec match	Inert. μ	Copr μ
SXS:BBH:0088	SXS:BBH:2519	0.0239	0.00837
SXS:BBH:0088	SXS:BBH:2580	0.0559	0.0388
SXS:BBH:3974	SXS:BBH:2581	0.0752	0.0324

TABLE III. Mismatches between eccentric precessing and eccentric non-precessing matching waveforms in inertial and co-precessing frames.

in the inertial frame, and with the precessing waveforms untwisted to the co-precessing frame. The resulting mismatches are displayed in Table III. All the mismatches are decreased in the co-precessing frame. The mismatch for the SXS:BBH:0088 and SXS:BBH:2519 match is the lowest, and is on the order of 10^{-3}, indicating that the match is reasonably accurate.

We now walk through a more detailed investigation of the SXS:BBH:0088/ SXS:BBH:2519 match. We first untwist SXS:BBH:0088 into the co-precessing frame to compare it to its non-precessing counterpart. Figure 11 shows this comparison in the inertial and co-precessing frame, as well as a comparison of SXS:BBH:0088 itself

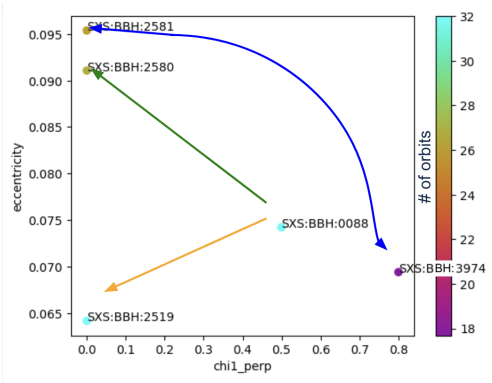

FIG. 12. $\chi_{1_\perp}$ vs. eccentricity with number of orbits colorbar for eccentric precessing and eccentric non-precessing NR simulation matches. Arrows show precessing/non-precessing matches. $\chi_{2_\perp}$ negligible for all waveforms.

between the two frames. From initial qualitative comparisons, the transformation drastically lessens precession effects, making it more similar to a non-precessing waveform. In particular, the cross polarization of the

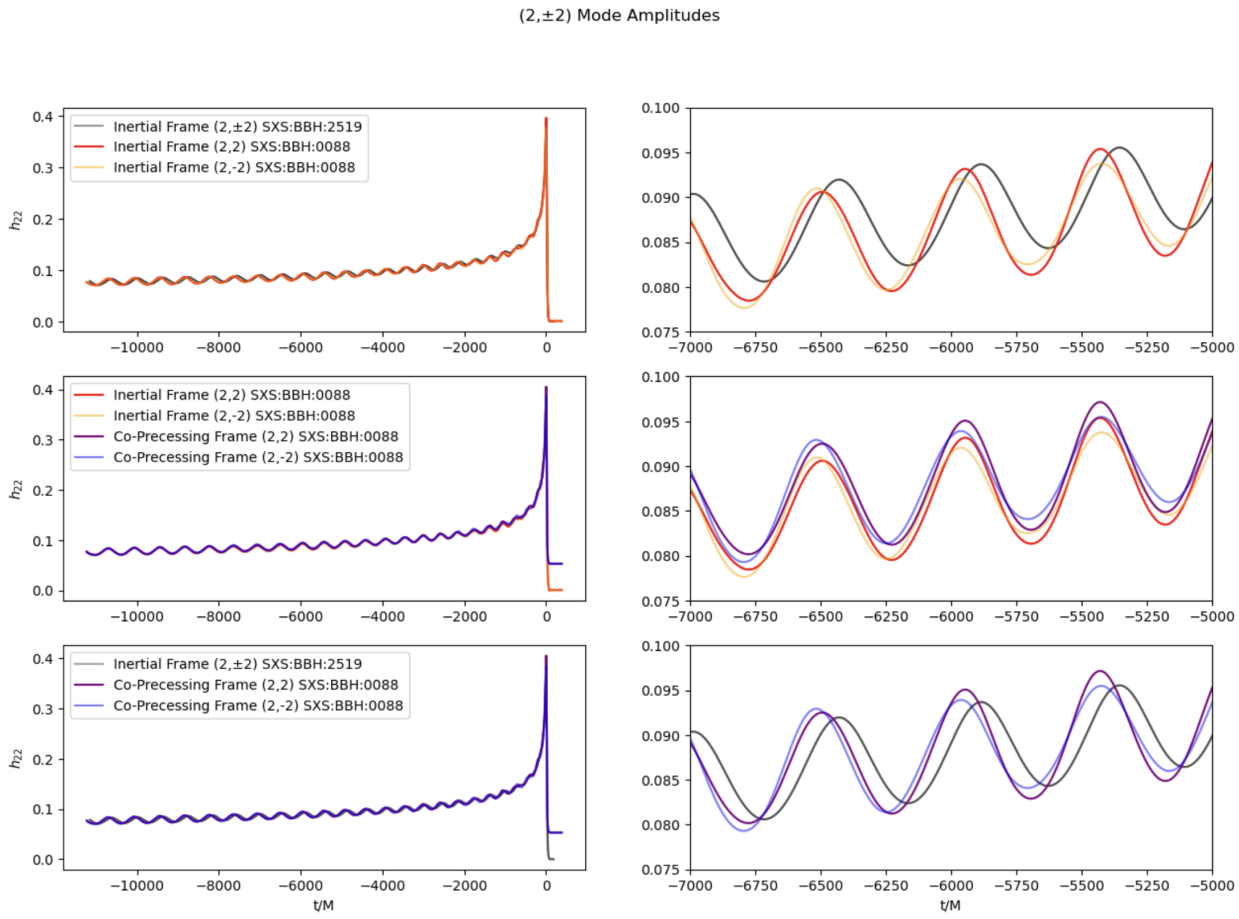

FIG. 13. (2,±2) mode amplitudes over time for eccentric precessing simulation SXS:BBH:0088 in the inertial and co-precessing frames and eccentric non-precessing simulation SXS:BBH:2519 in the inertial frame. The two mode amplitudes are the same for the non-precessing system. In both the inertial and co-precessing frames for the precessing system, the (2,2) and (2,-2) mode amplitudes are offset from each other in phase and amplitude, displaying that the mode asymmetry created by precession is not eliminated in the co-precessing frame. Waveforms accessed from the SXS catalog [14].

strain is much closer to zero than in the inertial frame (as also shown in Figure 10). However, small wiggles of modulating amplitude remain in the cross polarization of SXS:BBH:0088, unlike its non-precessing counterpart which has a completely flat cross polarization. These features cannot be explained by differences between the two waveforms' parameters, showing that the co-precessing frame does not completely erase precession effects.

To further investigate the differences between these waveforms, we plot comparisons of individual modes between SXS:BBH:0088 in the inertial frame and the co-precessing frame and SXS:BBH:2519 in the inertial frame (Figure 13). While the (2,±2) modes have the same amplitude for the non-precessing SXS:BBH:2519, indicating that mode symmetries are upheld, they are offset from each other in phase for SXS:BBH:0088 in both the inertial and co-precessing frames. In the inertial frame, this mode asymmetry is an effect caused by precession of the orbital plane. Its presence in the co-precessing frame indicates that this transformation does not remove mode asymmetries caused by precession, instead just shifting the envelope of the waveform upwards to be in line with that of a non-precessing system.

Though our initial hope was to do all our comparison plots using existing NR simulations, we are unable to due to the lack of matches within the catalog. To display why we could not relax our matching parameters to continue our analysis using just SXS simulations (without surrogates), in Figure 14 we plot a "bad match" created by loosening the requirement for similar orbital frequency. While the two waveforms have very similar eccentricities, spins, and mass ratios, their differing starting orbital frequencies leads the eccentric non-precessing SXS:BBH:2536 to be much longer than its counterpart. As a result, the plus polarizations of their strains are difficult to compare and only line up in brief sections of the plot. Thus, to enable a proper comparison it is necessary to have closely matching waveforms and loosening our matching criteria would interfere with our ability to evaluate the co-precessing frame. In order to proceed

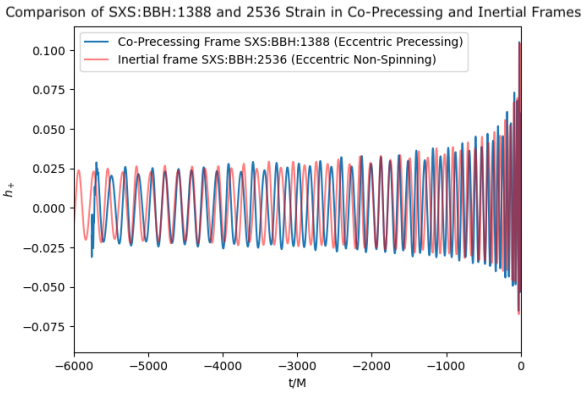

FIG. 14. Plus and cross polarization of strain over time for SXS:BBH:1388 (blue) in the co-precessing frame and SXS:BBH:2536 (red) in the inertial frame. The two waveforms line up at only a few points during their orbits, and the blue waveform is higher frequency than the red throughout. Waveforms accessed from SXS catalog [14].

with these comparisons, we will construct our own eccentric non-spinning waveforms with the same parameters as each eccentric precessing simulation from the SXS catalog.

D. Precessing NR vs. Generated SEOBNRv5EHM Matches

We begin creating non-precessing matches for the 27 eccentric precessing waveforms using waveform model SEOBNRv5EHM. To create these matches, we perform a mismatch minimization procedure that fits over starting orbital frequency and eccentricity until the time-domain mismatch of the (2,2) modes is at a minimum.

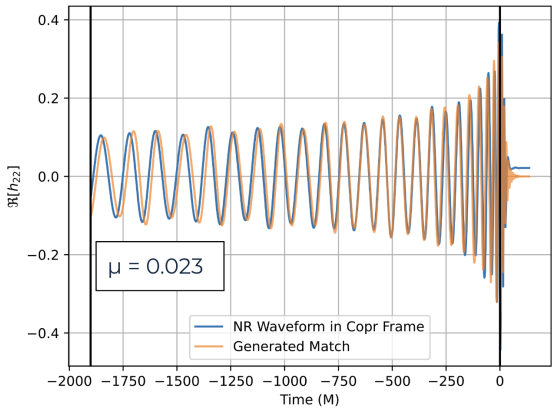

FIG. 15. (2,2) mode vs. time for NR eccentric precessing waveform in co-precessing frame and generated v5EHM match using mismatch minimization code. The mismatch between these waveforms is on the order of 10^{-2}. Waveforms accessed from SXS catalog [14] and created with SEOBv5EHM [15].

We then compare the eccentricities of the NR waveform and its match to determine if the co-precessing frame transformation effects eccentricity. This process has currently only been run on a few waveforms, one of which can be seen in Figure 15. For this waveform, eccentricity and starting orbital frequency are both slightly higher for the generated match. However, differences in initial parameters may be explained by the fact that the definition of eccentricity used differs between the SXS simulations and v5EHM code. To truly compare the dynamics (eccentricity, frequency, spins, etc.) of the systems, we will need to use another Python code called gweccentricity [17]. This package will ensure that we have a standardized definition of eccentricity and other dynamics by computing them directly from the NR and v5EHM waveforms, rather than the input parameters.

V. CHALLENGES AND FUTURE STEPS

Our results indicate first that scri can correctly find co-precessing frame regardless of effects from eccentricity in isolation, as confirmed by our mismatches of non-precessing waveforms in the inertial and co-precessing frame. Additionally, we confirm that the co-precessing frame removes many precession effects and more closely approximates a non-precessing waveform, but note some lingering precession effects and in particular confirm that mode asymmetries are not removed by the co-precessing frame transformation. We begin an analysis of changes to waveform eccentricity and other dynamics using SEOBv5EHM matches to the 27 NR eccentric precessing waveforms, with no firm conclusions as of yet.

Moving forward, we will continue to generate SEOBv5EHM matches for the 27 eccentric precessing NR waveforms, and use gweccentricity [17] to analyze the differences in their dynamics. In particular, we hope to continue to study differences in eccentricity over time between the eccentric precessing untwisted and just eccentric waveforms to determine if the co-precessing frame approximation affects eccentricity estimations of a waveform. For these matches, we will update our mismatch minimization procedure to include higher order modes rather than matching on solely the (2,2) mode. We will also continue to investigate mode asymmetries and other precession-related features that are not affected by the co-precessing frame transformation.

VI. ACKNOWLEDGMENTS

I would like to thank my mentors Lucy Thomas and Taylor Knapp for all their guidance and support throughout this project. I would also like to gratefully acknowledge the U.S. National Science Foundation, Caltech Student-Faculty Programs, and the LIGO Summer Undergraduate Research Fellowship.

[1] LIGO Scientific Collaboration, Virgo Collaboration, and KAGRA Collaboration, LVK Algorithm Library - LALSuite, Free software (GPL) (2018).

[2] M. Mapelli, Binary black hole mergers: Formation and populations, Frontiers in Astronomy and Space Sciences **7**, 10.3389/fspas.2020.00038 (2020).

[3] M. Favata, SXS, and K. Thorne, Elliptical binaries, Sounds of Spacetime (2025).

[4] T. A. Apostolatos, C. Cutler, G. J. Sussman, and K. S. Thorne, Spin-induced orbital precession and its modulation of the gravitational waveforms from merging binaries, Phys. Rev. D **49**, 6274 (1994).

[5] M. Favata, SXS, and K. Thorne, Spinning binaries, Sounds of Spacetime (2025).

[6] P. Schmidt, M. Hannam, and S. Husa, Towards models of gravitational waveforms from generic binaries: A simple approximate mapping between precessing and non-precessing inspiral signals, Phys. Rev. D **86**, 104063 (2012), arXiv:1207.3088 [gr-qc].

[7] M. A. Shaikh, V. Varma, A. Ramos-Buades, H. P. Pfeiffer, M. Boyle, L. E. Kidder, and M. A. Scheel, Defining eccentricity for spin-precessing binaries (2025), arXiv:2507.08345 [gr-qc].

[8] M. Boyle, L. E. Kidder, S. Ossokine, and H. P. Pfeiffer, Gravitational-wave modes from precessing black-hole binaries (2014), arXiv:1409.4431 [gr-qc].

[9] P. Schmidt, M. Hannam, S. Husa, and P. Ajith, Tracking the precession of compact binaries from their gravitational-wave signal, Phys. Rev. D **84**, 024046 (2011).

[10] R. O'Shaughnessy, B. Vaishnav, J. Healy, Z. Meeks, and D. Shoemaker, Efficient asymptotic frame selection for binary black hole spacetimes using asymptotic radiation, Physical Review D **84**, 10.1103/physrevd.84.124002 (2011).

[11] M. Boyle, Angular velocity of gravitational radiation from precessing binaries and the corotating frame, Physical Review D **87**, 10.1103/physrevd.87.104006 (2013).

[12] M. Boyle, R. Owen, and H. P. Pfeiffer, Geometric approach to the precession of compact binaries, Physical Review D **84**, 10.1103/physrevd.84.124011 (2011).

[13] S. Albanesi, R. Gamba, S. Bernuzzi, J. Fontbuté, A. Gonzalez, and A. Nagar, Effective-one-body modeling for generic compact binaries with arbitrary orbits (2025), arXiv:2503.14580 [gr-qc].

[14] The sxs catalog of simulations (2025).

[15] A. Gamboa *et al.*, Accurate waveforms for eccentric, aligned-spin binary black holes: The multipolar effective-one-body model SEOBNRv5EHM, (2024), arXiv:2412.12823 [gr-qc].

[16] K. S. Phukon, N. K. Johnson-McDaniel, A. Singh, and A. Gupta, Evolution of precessing binary black holes on eccentric orbits using orbit-averaged evolution equations, (2025), arXiv:2504.20543 [gr-qc].

[17] M. A. Shaikh, V. Varma, H. P. Pfeiffer, A. Ramos-Buades, and M. van de Meent, Defining eccentricity for gravitational wave astronomy, Physical Review D **108**, 10.1103/physrevd.108.104007 (2023).